Journal of Cultural Heritage 55 (2022) 221–227

Contents lists available at ScienceDirect

Journal of Cultural Heritage

journal homepage: www.elsevier.com/locate/culher

Original article

Complementary analysis to de-convolute co-located contaminants in marine archaeological bricks

Rebecca Grethe[a], Kevin J.W. Etherdo-Sibley[b], Chiu Tang[c], Sarah Day[c], Donna C. Arnold[b,*], Eleanor Schofield[d,*]

[a] Landesmuseum Hannover, Willy-Brandt-Allee 5, Hannover 30169, Germany
[b] School of Physical Sciences, University of Kent, Canterbury, CT2 7NH, UK
[c] Diamond House, Harwell Science and Innovation Campus, Fermi Ave, Didcot OX11 0DE, UK
[d] Mary Rose Trust, HM Naval Base, Portsmouth, PO1 3LX, UK

ARTICLE INFO

Article history:
Received 30 September 2021
Accepted 28 February 2022

Keywords:
Archaeological bricks
Conservation
Mary Rose
Scanning electron microscopy – energy dispersive spectroscopy
X-ray powder diffraction
Synchrotron techniques

ABSTRACT

Marine archaeological artefacts contain unexpected compounds due to prolonged exposure to the sea. These can remain dormant and embedded within materials until a change in their surrounding environment, such as exposure to oxygen, prompts a transformation. These changes can pose a problem, as acidic compounds are formed which disintegrate the material, or crystals form which physically break the artefact apart. The extent of these transformations is highly heterogeneous due to its dependence on the ability for oxygen to reach and catalyse these reactions. Additionally, these transformations are heavily dependent on the environment the artefact is exposed to, and the pathways available for ingress, either naturally or through previous degradation. This results in materials with a range of different compounds which are often co-located on the macro, micro and nano-scale. Trying to de-convolute these compounds is challenging, and usually requires a suite of complementary techniques to achieve. Here we report on damaging salts found within marine archaeological bricks and show how it is only possible to qualitatively and quantitatively understand what is present by employing a range of analytical techniques, such as XRD, SEM-EDS and SR-XPD. The marine archaeological bricks studied were found to contain a range of different sulfate-based salts, which had grown crystals in preferred orientations. This provides information which will guide further conservation strategies such as how these bricks are stored, conserved and protected in the future.

Introduction

A wealth of cultural heritage can be found in the depths of our seas and oceans. Their preservation is usually attributed to the accumulation of protective layers of silt, which act as a barrier to oxygen. This disables typical degradation mechanisms, such as the corrosion of metals or the activity of organisms which degrade organic materials. In most cases some damage has occurred prior to discovery, making the development of conservation strategies post-excavation crucial to their long-term survival. These measures usually act to initially remove any debris via cascade washing, followed by stabilisation treatments, where necessary. Whilst seemingly stable, it is common for conservation problems to arise in subsequent years due to the activity of unknown entities lurking beneath the surface of the object, and their transformation in changing surrounding environments.

Porous objects that have spent significant years in the marine environment will inevitably incorporate some of the elements and compounds surrounding them. These can originate from the seawater (e.g. sulfur, iron, magnesium, sodium, chlorine etc.), corrosion products from metallic artefacts which did not survive in the sewater, or a mixture thereof. Sometimes the chemical state these compounds exist in upon excavation present little threat to the stability of the object, and may not be dislodged by cascade water washes that are typically used to remove foreign entities. Therefore, they remain invisible until external conditions provoke

Abbreviations: SEM-EDS, scanning electron microscopy – energy dispersive spectroscopy; XRD, X-ray diffraction; SR-XPD, synchrotron radiation - X-ray powder diffraction.

* Corresponding authors.
E-mail addresses: d.c.arnold@kent.ac.uk (D.C. Arnold), e.schofield@maryrose.org (E. Schofield).

https://doi.org/10.1016/j.culher.2022.02.013

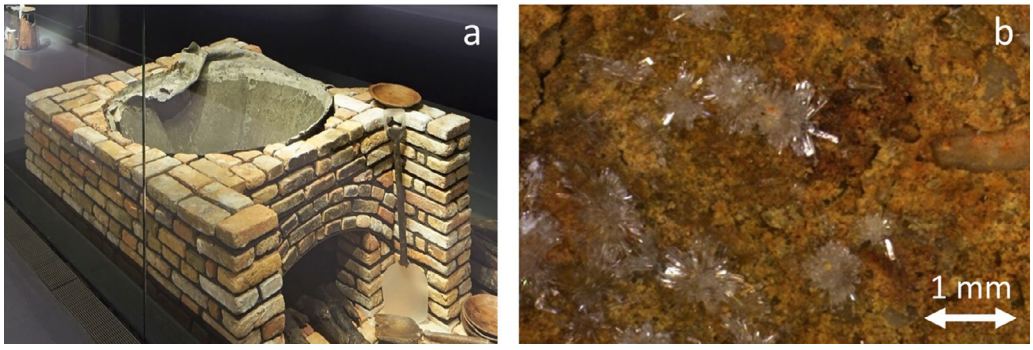

Fig. 1. (a) The *Mary Rose* brick oven on display at the museum (b) Light microscope image of salts on *Mary Rose* brick.

a chemical change. Furthermore, the extent to which these compounds are included within an object increases with the natural or degradation induced porosity of the object.

The evolution of an object post active conservation has been well documented for marine archaeological iron and wood [1–3]. In the former, residual chloride containing species accelerate the formation of damaging corrosion products, resulting in irreparable damage [4–6]. In the latter, these manifest as damaging salts which can both mechanically and chemically compromise the wood [1,2,7,8]. These salts are attributed to sulfur, whose inclusion can be traced back to the seawater where abundantly available sulfate can be biogenically reduced, and form compounds such as Pyrite and Greigite, amongst others. When excavated the compounds are present in a reduced form, which would likely have been impervious to a cascade water wash, and therefore remained within the wood. It has been shown that exposure to oxygen will cause these to oxidise and degrade the remaining wood [8]. The detection of these compounds in marine archaeological wood highlights the likelihood of similar products being found in any other porous archaeological materials removed from such an environment.

The *Mary Rose* collection, from the excavated flagship of Henry VIII's, has a range of both inorganic and organic materials [9,10]. Between 1981 and 1983, over 3000 bricks were excavated from the fireplace in the ship's galley (Fig. 1a). Initial conservation efforts involved a cascade water wash, to remove sodium chloride, followed by controlled drying. After over 30 years of storage and display, the bricks face a new threat, as the formation of salts has become visible (Fig. 1b).

Salts can be discriminated into two groups: soluble and insoluble, with the latter usually less of a concern in artefacts. In contrast, soluble salts can be particularly damaging due to changes in relative humidity (RH) promoting their repeated and cycling deliquescence and recrystallization. At higher RH the salts absorb moisture to form a solution, but conversely at lower RH the salts dry out and recrystallize. During these cycles the salts can grow within the vacancies in porous materials to such a size that they physically break the item, causing irreversible damage. This can be partly mitigated by storing in controlled environments (e.g. RH below the point of deliquescence). However, this usually reduces rather than eliminates the problem. Additionally, this requires a full understanding of the phases present such that optimal conditions can be identified and maintained.

Whilst there have been numerous studies into salt weathering of terrestrial bricks and stone [11–15], there is little on post-conservation threats faced by bricks or ceramic materials which have been retrieved from the marine environment, and have undergone a conservation treatment. To understand the threat posed to these unique materials and the potential impact on their long-term stability, it is imperative to elucidate the compounds present. Here we present a comprehensive examination of salts forming on and within marine archaeological bricks.

Research aim

The aim of this research is to determine what compounds are present in marine archaeological bricks, post conservation. Traditional conservation methods will have only removed the compounds that the solution of choice is reactive to. Therefore, anything left behind remains a potential threat in the future, especially if they are compounds that will react to a changing environment e.g. temperature and/or humidity. The threat of sulfur containing compounds in marine archaeological wood is well identified, however the same cannot be said for archaeological brick. This is likely as it is an inorganic material and thought less susceptive to change, and damage. However, cycling moisture content in the air will cause rapid change in the sulfur compounds, with potentially devastating consequences. In order to determine the scale of the problem, and devise treatments to remove the problem compounds and/or determine suitable storage conditions which would ensure their safety, understanding exactly what compounds are present is critical. A suite of techniques were used to achieve this, from visual inspection to detailed elemental and crystal structure analysis.

Materials & methods

Sample preparation

A set of 20 bricks from the *Mary Rose* collection that visibly had salts forming on them, were selected for analysis. These could be seen with the naked eye and further examination using light microscopy gave a qualitative indication of some of the crystal morphologies present (Fig. 1b). Samples were taken from brick parts that were broken off due to salt damage, as well as from salts which had completely flaked off the brick. For EDS analysis, the salts were pressed into pellets. Where the collected amount of salt was not sufficient, cellulose was added as a filler (this resulted in 14 salt pellet samples). Small parts of the brick samples were ground and also pressed into pellets for bulk analysis. The brick powder was mixed with cellulose to avoid disintegration of the pellet. Samples were ground in a mortar for XRD-analysis.

Light microscopy

A Zeiss SmartZoom light microscope was used for analysis.

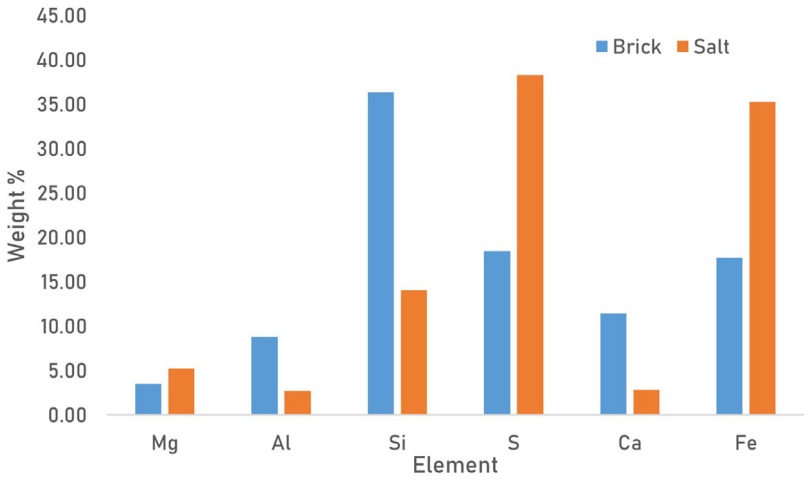

Fig. 2. SEM-EDS analysis of salt & brick samples from 14 bricks.

SEM-EDS analysis

Brick and salt pellet samples were observed with a Scanning electron microscope (SEM) (Jeol 5510) and analysed using the coupled Electron-dispersive X-ray spectroscopy (EDS) (XMax, Oxford instruments), operating at 20 kV. Collection time was 120 s. Elemental mapping of salts and brick surfaces (not pressed into pellets) was performed for selected samples.

pH testing

To test the acidity of the salts, 0.05 g of each sample were mixed with 10 mL of deionised water respectively. The pH of the solutions was measured daily using pH paper.

XRD and SR-XRD

X-ray diffraction (XRD) data were collected using the Panalytical XPert [3] diffractometer using a Cu target ($\lambda = 1.5406$ Å) and operating at 40 mA and 40 kV. Data were collected for approximately 2 h over a 2θ range of 5°–80° with a step size of 0.017° and a count time of 2 s/step. Phase analysis was performed using the search-match function in the Highscore software [16]. These analyses were performed by restricting the search parameters to those elements observed in the EDS measurements.

Synchrotron data were collected on the I11 high-resolution powder diffractometer at the Diamond Light Source (UK). Data were collected in flat plate geometry with the samples held in place with Kapton film over a 2θ range of ~2°–150° with $\lambda = 0.826559(1)$ Å and a zero point of 0.001434(4)° determined from the refinement of a Si standard. Refinements were performed for the 82A0584 sample as described in the results and discussion using the GSAS suite of programs [17].

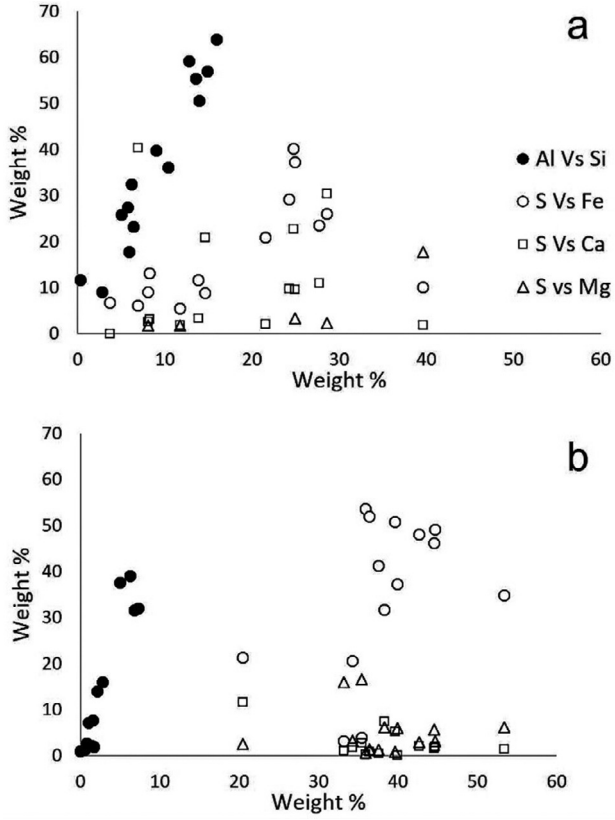

Fig. 3. Elemental correlations from SEM-EDS analysis for (a) brick samples (b) salt samples.

Results & discussion

The EDS elemental analysis of the brick and salt pellet samples are given in Fig. 2 (data given in Table S1). The average elemental value from 20 brick samples and 14 salt samples is displayed. Importantly, no Cl was detected in any of the samples. Na is the lightest element that can be confidently quantitatively investigated using this technique. In these samples, only trace amounts (approximately 1 wt%) of Na was detected and therefore not included further in our analysis. This indicates the success of the original conservation treatment to eradicate NaCl. In both the salt and brick samples typical brick constituents such as Al, Si and Ca were detected, with significantly less present in the salt samples. Conversely in all samples Fe and S were abundantly found, but with significantly more detected in the salt sample. Low levels of Mg were detected in both the brick and the salt samples.

Correlations between key elements are given in Fig. 3. A clear correlation exists between Al and Si, consistent with the base materials the bricks were constructed from. This is observed in both the brick and salt samples, as is a weaker correlation between S and Fe. The relationship between S and Ca and then S and Mg is less obvious. The most scattered correlation is between S and Ca, which is likely due to Ca being present in both the base material and subsequent salts that are forming. The correlations also point

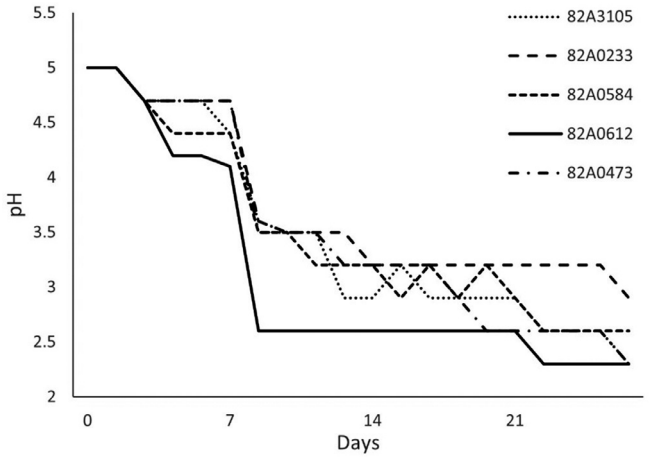

Fig. 4. . pH change in salts removed from brick and dissolved in deionised water

towards a mixture of species forming together, which is anticipated in complex heritage materials.

When the salts were put into deionised water, initially, no pH change was observed (Fig. 4). After two days, the pH in all samples decreased. After 7 days, a drastic decrease of the pH occurred. The pH of sample "*82A0612 salt*" dropped to 2.6 and the pH of all other samples decreased to between 3.5–3.6. A further decrease to a pH of 2.9–3.2 was observed in the following days for these samples. The pH of all sampled solutions then remained stable for the duration of the testing period.

This is explained by the presence of sulfuric acid and ferrous sulphate (iron(II)sulfate, $FeSO_4$) as a product of previous pyrite oxidation in elevated humidity as shown in the equation below:

$$2FeS_2 + 7O_2 + 2H_2O \rightarrow 2H_2SO_4 + 2FeSO_4$$

It then continues to form sulfuric acid and ferric sulphate (iron(III)sulphate, $Fe_2(SO_4)_3$ in the presence of water and oxygen:

$$4FeSO_4 + 2H_2SO_4 + O_2 \rightarrow 2Fe_2(SO_4)_3 + 2H_2O$$

This means that if the relative humidity in the storage is high and the salts absorb water, they create an acidic milieu within the bricks. This process is known to happen in archaeological wood from marine environments, as well as for pyrite in geological and fossil collections [18,19]

The sample solutions were dried slowly by lifting the lid of the sample containers. After a few days, crystal growth was observed. The recrystallised salts were then analysed by SEM-EDS (Fig. 5). The analyses showed the expected elements of Fe, S, and Ca. Small amounts of Si and Al were measured and attributed to residues of the brick material. The formation of two different crystal morphologies was observed, with different compositions. The one containing Ca and S produced long thin needles while the second was more compact and contained Fe and S. In some salts, the two species were found together but are clearly separable, visually and through EDS mapping (Figs. 5 and S1).

From the SEM-EDS and pH testing we can confirm that salts are forming which consist of Ca, S, and Fe. When recrystallizing, the calcium sulfate forms platelets, whereas the iron sulfate remains bulk, and these compounds can co-locate. In order to understand and elucidate the mechanisms of salt (re)crystallisation it is important to identify the phases present. X-ray diffraction (XRD) provides a way to enable phase analyses for crystalline materials. X-ray diffraction was performed on 14 powdered samples. Fig. 6. shows a comparison of the XRD data collected for a selection of these powders. Full XRD patterns for all samples are given in the electronic supplementary information (Fig. S2). It is clear from these data that all materials investigated contain similar crystalline phases with the relative phase mixtures of the components changing between samples.

Search-match experiments were performed using the Highscore software [16], restricting the elements searched to those present in the EDS measurements, with the addition of lighter elements which are not reliably detected using fluorescence techniques. In the vast majority of the samples the main phases present were identified as iron sulfate hydrate, calcium sulfate hydrate and silica (arising from the bricks themselves), consistent with the EDS data. A table of the main phases found are given in Table S2. We note in some cases that the samples were poorly crystalline and/or contained large amorphous contributions. Furthermore, the large Fe contributions lead to large amounts of fluorescence in the data collected for some samples which resulted in background drift. Additionally, a number of very weak peaks within the patterns remain unassigned due to difficulties in reliably extracting peak match information. The set-up of the diffractometer does not filter out either $CuK_{\alpha 2}$ or Cuk_{β} radiation. This results in broad peaks and the similarities between the crystal structures of the phases present results in a large degree of peak overlap. This can make phase identification difficult and precludes the possibility of unpicking potential cationic substitution or percentage phase contribution. At the identification stage, analysis is only qualitative. However, in order to monitor phase growth and to determine the efficacy of treatments, we need qualitative information, such as phase percentages. In order to more deeply investigate these materials, we performed synchrotron radiation experiments on the high resolution powder diffractometer (I11) at the Diamond Light Source (UK).

Fig. 7a shows a comparison between the XRD diffraction data collected for the 82A0584 sample compared with data collected on I11. Clear differences exist between the two patterns. However, these can be seen to be linked to the higher resolution and improved signal to noise afforded by synchrotron experiments when compared with laboratory-based experiments. Additionally, it can be seen that the peaks in the synchrotron data are far sharper allowing for multiple peak contributions to be more easily resolved. This is primarily due to the monochromatic wavelength of the synchrotron radiation and higher resolution afforded by the multi-analyser crystal (MAC) detector set-up. As with the XRD data, it is clear from the comparison of the data collected (for the same five samples shown in Fig. 6) that whilst the intensities change due to varying phase percentages, the same phases are present across all samples (Fig. 7b).

To obtain a deeper understanding of these materials using synchrotron measurements we have further analysed the data collected for the 82A0584 material. Search-match analyses demonstrated the presence of $FeSO_4{\cdot}xH_2O$ and SiO_2 consistent with the analyses of the XRD data. Additionally, $CaSO_4{\cdot}4H_2O$ is also identified. However, as with XRD analyses, phase identification becomes difficult due to problems such as peak overlap, preferred orientation and limitations in the materials available in the search-match databases (JCPDS). Rietveld refinement allows for the modeling of the phases present, allows for peak overlap to be taken into account, and importantly determines phase percentages. We performed Rietveld refinements using the GSAS suite of programs for the 82A0584 sample [17]. With complex data such as those collected here, it is important to consider the post processing of data collected at the beamline. These data were binned with 5 different step sizes of 0.002°, 0.004°, 0.006°, 0.008° and 0.010°. Changing the binning conditions changes the number of points used to describe the data. A decrease in the number of points comes at the price of decreased resolution (see Fig. S3). In many Refinement programs, such as GSAS, there is an upper limit to the number

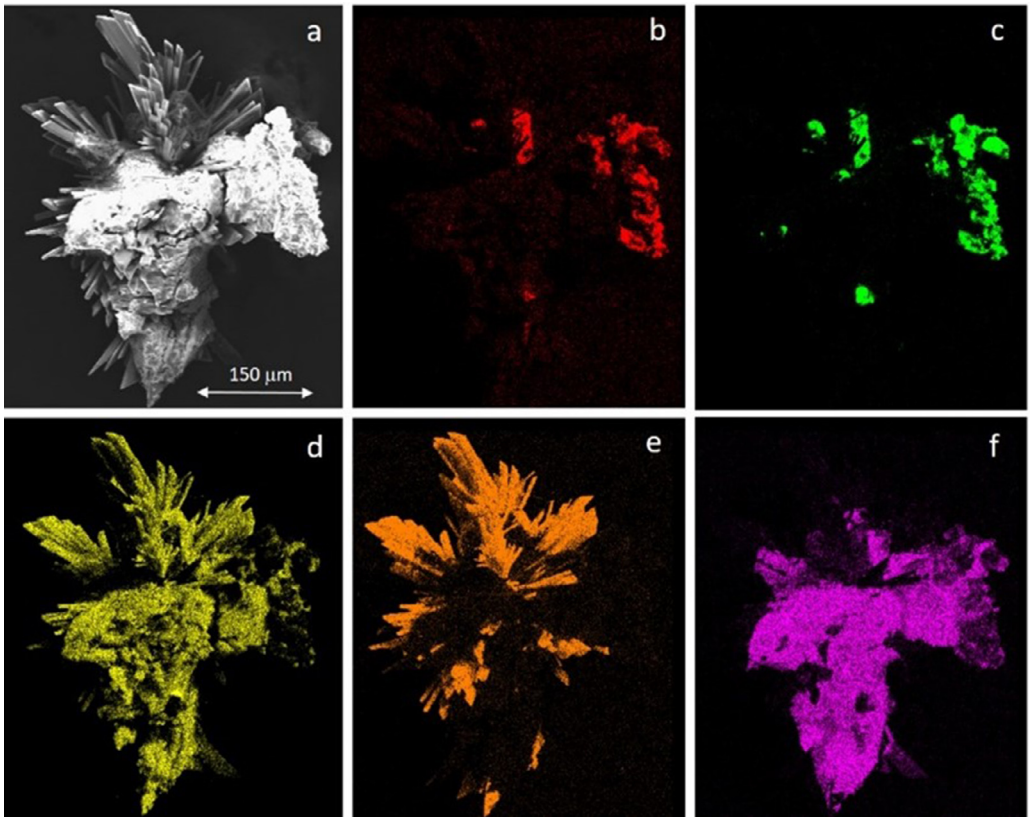

Fig. 5. (a) SEM image of recrystalised salt sample from brick 82A0584 with EDS mapping for (b) Al (c) Si (d) S (e) Ca (f) Fe.

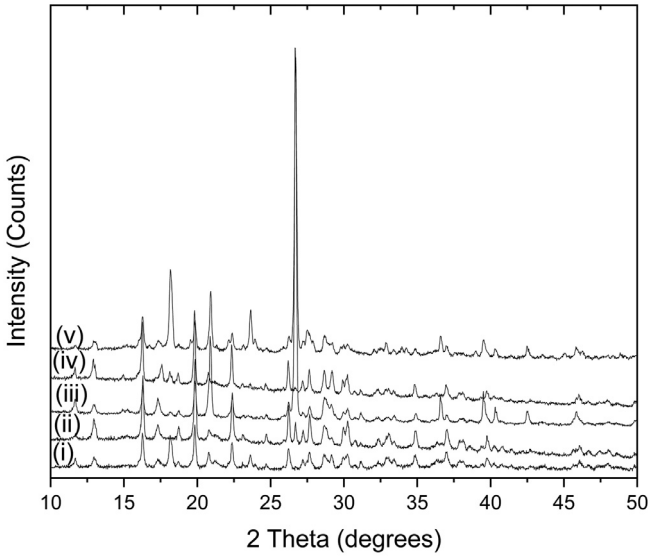

Fig. 6. X-ray diffraction data collected for (i) 82A0612, (ii) 82A3105, (iii) 82A0473, (iv) 82A0233 and (v) 82A0584 showing that whilst in differing amounts these materials largely contain the same components. Data shifted for clarity.

of data points that the program can physically process. Additionally, large numbers of data points can significantly slow the refinement process. This, coupled with complexities of performing multiphase refinements, can mean that the refinements become unresolvable due to correlations between physical parameters such as the lattice parameters, peak shape, atom positions etc. Lowering the number of data points can help speed up the refinement process but means there is less peak definition. This, in turn, limits the reliability when determining values for physical factors. For these refinements we used a binning size of 0.06°, which offers a balance between number of points and resolution allowing for refinement of the data. We have refined parameters such as lattice parameters, atom positions, peak shape and background. The parameters in each phase were refined singly (without the other phases included) in order to minimise correlations between parameters. The background was determined with 10 terms using a shifted Chebyschev polynomial function. The peak shape was modelled using the pseudo-Voigt function (type 2 in GSAS) described by Howard, and Thompson et al. [20,21]. Refinements were performed with four phases namely, SiO_2 [22], $FeSO_4{\cdot}7H_2O$ [23], $FeSO_4{\cdot}4H_2O$ [24] and $CaSO_4{\cdot}2H_2O$ [25]. Six spherical Harmonic order (ODF) terms were also refined in a cylindrical geometry for each phase in order to mitigate surface roughness/preferred orientation effects introduced by preparation of the sample for diffraction analysis. In all cases the Texture Index was close to 1, indicating that the sample is randomly orientated. Lattice parameters, phase percentages and goodness-of-fit parameters are given in Table 1 with the refinement profile given in Fig. 8a. There is a good fit between the models used and the data collected (Fig. 8). However, there remain peaks within the diffraction pattern which are not fit by these models, suggesting there are some small amounts of unidentified phases. Attempts to identify these phases through search-match and pattern matching using the Inorganic Chemistry Structural Database (ICSD) were unsuccessful. A deeper understanding of these materials and potential phase chemistries is required in order to be able to further explore candidate phases. Whilst we have only performed a single refinement we have translated this phase information on to the synchrotron data comparison plot originally shown in Fig. 7b to demonstrate that the changes in rel-

Table 1
Table giving space group, lattice parameters and phase percentages for the Rietveld refinement of 82A0584 using models for SiO_2[22], $FeSO_4{\cdot}7H_2O$[23], $FeSO_4{\cdot}4H_2O$[24] and $CaSO_4{\cdot}2H_2O$[25]]. Goodness-of-fit-parameters wRp = 12.80 % and Rp = 8.42 %.

Parameter	Phase			
	SiO_2	$FeSO_4{\cdot}7H_2O$	$FeSO_4{\cdot}4H_2O$	$CaSO_4{\cdot}2H_2O$
Space Group	$P3_221$	$P2_1/c$	$P2_1/n$	$I2/c$
a (Å)	4.90959(3)	14.048(2)	5.96324(8)	5.6735(5)
b (Å)	4.90959(3)	6.4949(8)	13.6050(1)	15.1886(1)
c (Å)	5.40049(6)	11.0285(9)	7.96242(8)	6.5320(6)
α (°)	90	90	90	90
β (°)	90	105.62(1)	90.499(1)	118.521(5)
γ (°)	120	90	90	90
Cell Volume (Å³)	112.734(2)	969.4(1)	645.97(1)	494.57(8)
Phase fraction	43.1(1)	24.3(3)	32.1(1)	0.49(4)

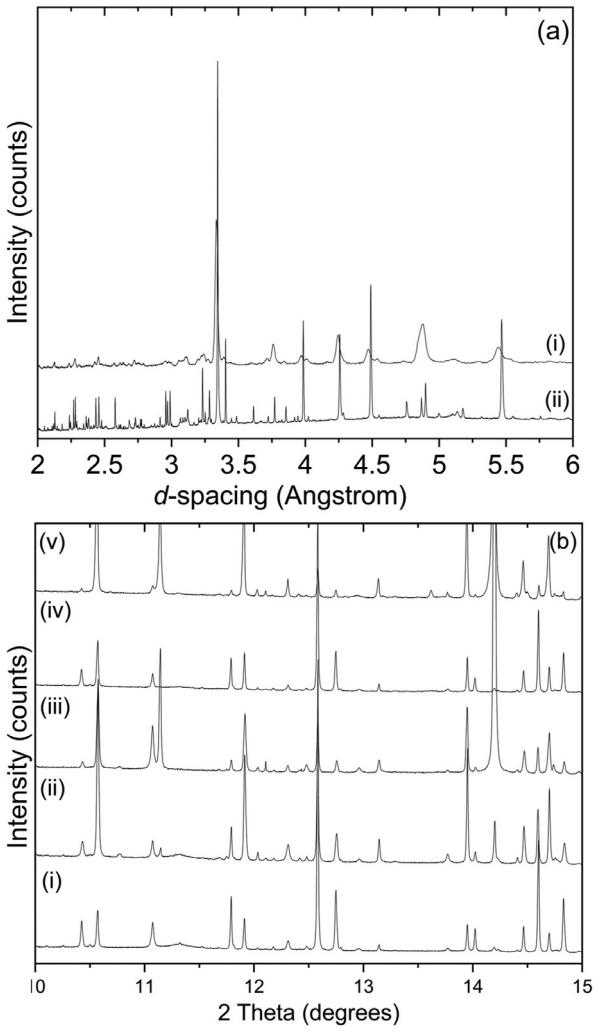

Fig. 7. (a) comparison of synchrotron (i) and X-ray diffraction (ii) data collected for 82A0584 showing increased intensity and improved resolution allowing additional peaks to be resolved and (b) comparison of the synchrotron data collected for (i) 82A0612, (ii) 82A3105, (iii) 82A0473, (iv) 82A0233 and (v) 82A0584 showing that these materials largely contain the same components. Data shifted for clarity.

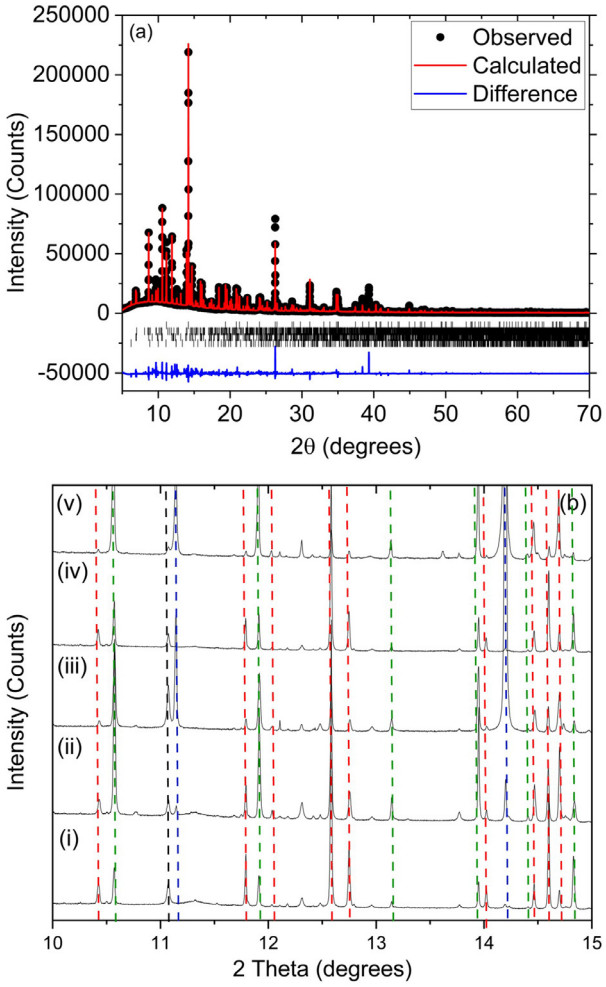

Fig. 8. (a) Rietveld refinement for the SR-XPD data collected for 82A0584 where the black circles are the observed dates, the red line is the fit to the model and the blue line is the difference curve. The black tick marks show where peaks are predicted from top to bottom for SiO_2, $FeSO_4{\cdot}7H_2O$, $FeSO_4{\cdot}4H_2O$ and $CaSO_4{\cdot}2H_2O$ respectively. (b) comparison of the synchrotron data collected for (i) 82A0612, (ii) 82A3105, (iii)_82A0473, (iv) 82A0233 and (v) 82A0584 showing the peaks attributable to SiO_2 (blue), $FeSO_4{\cdot}7H_2O$ (red), $FeSO_4{\cdot}4H_2O$ (green) and $CaSO_4{\cdot}2H_2O$ (black) respectively. Data shifted for clarity.

ative peak intensities are linked to changes in relative phase percentages (Fig. 8b). This highlights the potential to extract meaningful quantitative data from complex materials which will allow us to follow treatment protocols, understand their processes, and crucially demonstrate that they are working to remove/limit the growth of damaging salts.

Conclusions

Compounds present in marine archaeological bricks post excavation and active conservation, can rapidly change and form highly acidic and therefore damaging products. A suite of techniques, from visual inspection to elemental analysis and crystal structure studies, were performed to gain a better understanding on what is present and the scale of the threat they pose. The complexity of studying these materials was highlighted by the inability to gain meaningful information from laboratory based XRD, both in terms of phase identification and quantification. To alleviate this, synchrotron-based techniques were employed. However, complications still arose from peak overlap due to the number of compounds present. Powder XRD data confirmed the presence of Fe and Ca salts along with SiO_2 from the bricks themselves.

Being able to determine accurate phase compositions and percentages is important if we are to develop treatment and display protocols such that we can mitigate damage to the bricks. Whilst complex, we have demonstrated that it is possible to get quantitative phase percentages from the Rietveld refinement of synchrotron data. However, these data have also allowed us to resolve many more phases present than initially identified in laboratory based XRD experiments. Identifying all phases present has proved difficult and further work is required to understand the origins of these phases (i.e. part of the parent brick composition or other aggressive phases requiring conservation against). This work represents the first steps towards developing a deeper understanding of these materials and the hidden threats which lie within them. Critical, if we are to store, display and develop protection methodologies to ensure the integrity of these heritage materials.

Funding

This research did not receive any specific grant from funding agencies in the public, commercial, or not-for-profit sectors.

Acknowledgments

Zeiss Microscopy for use of the SmartZoom to analyse the salts, particularly Stephen Furzeland and Matthew Tuttiett.

Diamond Light Source for allocation of beamtime on beamline I11 (proposal number CY24092).

David Pearson from Mary Rose Trust for assistance with sampling of the bricks.

Erasmus+ for supporting the placement of Rebecca Grethe at the Mary Rose Trust.

Supplementary materials

Supplementary material associated with this article can be found, in the online version, at doi:10.1016/j.culher.2022.02.013.

References

[1] M. Sandstrom, F. Jalilehvand, E. Damian, Y. Fors, U. Gelius, M. Jones, M. Salome, Sulfur accumulation in the timbers of King Henry VIII's warship Mary Rose: a pathway in the sulfur cycle of conservation concern, Proc. Natl. Acad. Sci. U. S. A. 102 (40) (2005) 14165–14170, doi:10.1073/pnas.0504490102.

[2] M. Sandström, F. Jalilehvand, I. Persson, U. Gelius, P. Frank, I. Hall-Roth, Deterioration of the Seventeenth-Century Warship Vasa by internal formation of sulphuric acid, Nature 415 (6874) (2002) 893–897, doi:10.1038/415893a.

[3] E.J. Schofield, Illuminating the past: X-ray analysis of our cultural heritage, Nat. Rev. Mater. 3 (9) (2018) 285–287, doi:10.1038/s41578-018-0037-4.

[4] M. Rimmer, D. Watkinson, Q. Wang, The impact of chloride desalination on the corrosion rate of archaeological iron, Stud. Conserv. 58 (4) (2013) 326–337, doi:10.1179/2047058412Y.0000000068.

[5] D.E. Watkinson, N.J. Emmerson, The impact of aqueous washing on the ability of BFeOOH to corrode iron, Environ. Sci. Pollut. Res. 24 (3) (2017) 2138–2149, doi:10.1007/s11356-016-6749-3.

[6] H. Simon, G. Cibin, P. Robbins, S. Day, C. Tang, I. Freestone, E. Schofield, A synchrotron-based study of the Mary Rose iron cannonballs, Angew. Chem. Int. Ed. 57 (25) (2018) 7390–7395, doi:10.1002/anie.201713120.

[7] K.M. Wetherall, R.M. Moss, A.M. Jones, A.D. Smith, T. Skinner, D.M. Pickup, S.W. Goatham, A.V. Chadwick, R.J. Newport, Sulfur and Iron speciation in recently recovered timbers of the Mary Rose revealed via X-ray absorption spectroscopy, J. Archaeol. Sci. 35 (5) (2008) 1317–1328, doi:10.1016/j.jas.2007.09.007.

[8] E.R. Aluri, C. Reynaud, H. Bardas, E. Piva, G. Cibin, J.F.W. Mosselmans, A.V. Chadwick, E.J. Schofield, The formation of chemical degraders during the conservation of a wooden tudor shipwreck, ChemPlusChem 85 (8) (2020) 1632–1638, doi:10.1002/cplu.202000160.

[9] P. Marsden, Sealed by Time: The Loss and Recovery of the Mary Rose, 1st ed., Mary Rose Trust, 2003.

[10] M.A. Jones, For Future Generations: Conservation of a Tudor Maritime Collection, Mary Rose Trust, 2011.

[11] H. Morillas, C. Garcia-Florentino, I. Marcaida, M. Maguregui, G. Arana, L.F.O. Silva, J. Manuel Madariaga, *In-situ* analytical study of bricks exposed to marine environment using hand-held X-ray fluorescence spectrometry and related laboratory techniques, Spectrochim. Acta Part B At. Spectrosc. 146 (2018) 28–35, doi:10.1016/j.sab.2018.04.020.

[12] H. Morillas, F.F. de Mendonça Filho, H. Derluyn, M. Maguregui, D. Grégoire, J.M. Madariaga, Decay processes in buildings close to the sea induced by marine aerosol: salt depositions inside construction materials, Sci. Total Environ. 721 (2020) 137687, doi:10.1016/j.scitotenv.2020.137687.

[13] C. Scatigno, N. Prieto-Taboada, M. Preite Martinez, A.M. Conte, J.M. Madariaga, A non-invasive spectroscopic study to evaluate both technological features and conservation state of two types of ancient roman coloured bricks, Spectrochim. Acta Part A Mol. Biomol. Spectrosc. 204 (2018) 55–63, doi:10.1016/j.saa.2018.06.023.

[14] C. Scatigno, N. Prieto-Taboada, G. Fiesta, J.M. Madariaga, Soluble salts quantitative characterization and thermodynamic modeling on roman bricks to assess the origin of their formation, Molecules 26 (2021) 2866.

[15] L. Germiario, C.T. Oguchi, Underground salt weathering of heritage stone: lithological and environmental constraints on the formation of sulfate efflorescences and crusts, J. Cult. Herit. 49 (2021) 85–93.

[16] T. Degen, M. Sadki, E. Bron, U. Konig, G. Nenert, The highscore suite, Powder Diffr. 29 (S2) (2014) S13–S18.

[17] A.C. Larson, R.B. Von Dreele, Los Alamos Natinoal Report LAUR. 96 (1994) 86–748.

[18] C. Rémazeilles, K. Tran, E. Guilminot, E. Conforto, P. Refait, Study of Fe(II) sulphides in waterlogged archaeological wood, Stud. Conserv. 58 (4) (2013) 297–307, doi:10.1179/2047058412Y.0000000071.

[19] L. Ratcliffe, A. Valentine-Baars, Investigative conservation of the Royal Cornwall Museum minerals, Geol. Curator 9 (5) (2011) 305–314.

[20] C.J. Howard, The approximation of asymmetric neutron powder diffraction peaks by Sums of Gaussians, J. Appl. Crystallogr. 15 (1982) 615–620.

[21] P. Thompson, D.E. Cox, J.B. Hastings, Rietveld refinement of Debye-Scherrer synchrotron X-ray data from Al_2O_3, J. Appl. Crystallogr. 20 (1987) 79–83.

[22] H. D'Amour, W. Denner, H. Schulz, Structure determination of α-Quartz up to 68 x 108 Pa, Acta Crystallogr. Sect. B 35 (3) (1979) 550–555.

[23] W.H. Baur, On the crystal chemistry of salt hydrates. III. the determination of the crystal structure of $FeSO_4.7H_2O$ (Melanterite), Acta Crystallogr. 17 (1964) 1167–1174.

[24] W.H. Baur, Zur kristallchemie der salzhydrate. Die kristallstrukturen von $MgSO_4.4H_2O$ (Leonhardtit) Und $FeSO_4.4H_2O$ (Rozenit), Acta Crystallogr. 15 (1962) 815–826.

[25] W.F. Cole, C.J. Lancucki, A refinement of the crystal structure of gypsum $CaSO_4.2H_2O$, Acta Crystallogr. Sect. B 30 (4) (1974) 921–929.